

RESEARCH ARTICLE

A 3D-Printed Oxygen Control Insert for a 24-Well Plate

Martin D. Brennan, Megan L. Rexius-Hall, David T. Eddington*

Dept of Bioengineering, University of Illinois at Chicago, Chicago, Illinois, United States of America

* dte@uic.edu



OPEN ACCESS

Citation: Brennan MD, Rexius-Hall ML, Eddington DT (2015) A 3D-Printed Oxygen Control Insert for a 24-Well Plate. PLoS ONE 10(9): e0137631. doi:10.1371/journal.pone.0137631

Academic Editor: Arum Han, Texas A&M University, UNITED STATES

Received: April 24, 2015

Accepted: August 19, 2015

Published: September 11, 2015

Copyright: This is an open access article, free of all copyright, and may be freely reproduced, distributed, transmitted, modified, built upon, or otherwise used by anyone for any lawful purpose. The work is made available under the [Creative Commons CC0](https://creativecommons.org/licenses/by/4.0/) public domain dedication.

Data Availability Statement: The authors confirm that all data underlying the findings are fully available without restriction. All data for the paper is presented within it and the supporting information.

Comprehensive documentation including the 3D cad files are held in the project repository on Github (<https://github.com/Biological-Microsystems-Laboratory/3d-printed-oxygen-control-insert>).

Funding: This work was supported by National Science Foundation 1253060, DTE (http://www.nsf.gov/awardsearch/showAward?AWD_ID=1253060). The funders had no role in study design, data collection and analysis, decision to publish, or preparation of the manuscript.

Abstract

3D printing has emerged as a method for directly printing complete microfluidic devices, although printing materials have been limited to oxygen-impermeable materials. We demonstrate the addition of gas permeable PDMS (Polydimethylsiloxane) membranes to 3D-printed microfluidic devices as a means to enable oxygen control cell culture studies. The incorporation of a 3D-printed device and gas-permeable membranes was demonstrated on a 24-well oxygen control device for standard multiwell plates. The direct printing allows integrated distribution channels and device geometries not possible with traditional planar lithography. With this device, four different oxygen conditions were able to be controlled, and six wells were maintained under each oxygen condition. We demonstrate enhanced transcription of the gene VEGFA (vascular endothelial growth factor A) with decreasing oxygen levels in human lung adenocarcinoma cells. This is the first 3D-printed device incorporating gas permeable membranes to facilitate oxygen control in cell culture.

Introduction

Here we report on the development of 3D-printed microfluidic devices for the control of oxygen in cell culture microenvironments. We demonstrate a device that nests into a 24-well culture plate to control gas in each row of the plate independently of the incubator's condition. This expands on our previous work of a device fabricated using PDMS molds and planar lithography for 6-well plates [1, 2]. The ability to independently control oxygen across each row of the plate enables more efficient experiments as a separate incubator or hypoxic chamber is not needed for each condition.

3D printing of microfluidic devices enables rapid, one-step fabrication of complex designs infeasible to make with planar lithography and replica molding techniques [3, 4]. In addition, planar lithography is time consuming, requires specialized equipment and facilities, and has a high failure rate. It is not unusual for microfluidic labs to make ten microfluidic devices to guarantee one will work properly. On the other hand, 3D CAD printing allows for unambiguous specifications and nearly eliminates time and effort spent on fabrication which may be outsourced to a 3D printing company for around \$200/device [5]. 3D printing also allows integration of complex geometries not possible with planar lithography, such as hose barbs and

Competing Interests: The authors have declared that no competing interests exist.

luer fittings. Dissemination and distributed production is also vastly simplified due to easy sharing of the design as a CAD file. Due to these inherent advantages 3D printing has emerged as a method for directly printing complete microfluidic devices [5–9]. Many prototypical microfluidic device features have been recreated with 3D printing as a proof of concept for this new fabrication technique [5, 8] including modular re-configurable units [9–11]. 3D printed devices have been used for neuroengineering applications [12], inexpensive and high-throughput reactionware, [13–16], culturing and imaging arrays of seedlings [17], measuring dopamine and ATP levels in biological samples with an integrated electrode [18], or plate reader [7], and a bacteria separation flow assay [19, 20]. Other 3D-printed fluidic devices include pneumatic valves [21] a custom NMR cell [22], a rapid reconstitution package for lyophilized drugs [23] and flow plates for a water electrolysis system [24].

Printing is currently limited in choice of substrate compatible with the 3D printing process. Substrate options include many proprietary formulations which have been successfully used in a variety of applications. New techniques for using 3D-printed molds to produce devices [25–29] are also being developed, including fugitive ink methods [30–32]. To date, there are no widely available methods or materials to facilitate direct printing of gas-permeable materials, although this area is actively being explored [33]. Microfluidic cell culture devices are most commonly cast in PDMS as it is a convenient material for cell studies due to its biocompatibility, optical properties, and gas permeability, facilitating oxygen control of cell environments [34, 35]. In this study, a larger 24 well version was developed and optimized which includes several key improvements over the previous 6-well version.

Oxygen control in cells studies is often overlooked by researchers, but important for mimicking conditions experienced by cells *in vivo*. Typically cell culture studies are performed at 21% oxygen, atmospheric oxygen conditions, although levels that cells experience *in vivo* are less than 21% [35]. For example, tumors are generally hypoxic as cancer cells rapidly outgrow their vasculature creating a poorly perfused, hypoxic inner region [36]. Studying cancer cells under controlled hypoxic conditions is important in understanding the pathophysiology because research has shown hypoxia may enhance aggressive phenotypes, tumor progression, metastasis, and resistance to therapy [37–39]. Hypoxia is known to alter the transcription of many genes which are under the activity of the HIF (hypoxia inducible factor) family of transcriptional factors [40–42]. To better study the role of oxygen levels in cancer gene expression, a gas controlled culture system is required.

Previously, we developed multiwell inserts for 6-well plates that controlled oxygen in a standard off-the shelf well plate [1, 2]. These 6-well devices were completely cast from PDMS and fabricated in a multiple bonding procedure. In addition, tubing was used to connect each pillar which became quite cumbersome when moving to a newer 24-well version. Utilizing 3D printing for the fabrication allowed further features to be incorporated such as integrated distribution channels to eliminate the connection tubings between wells and hose barbs for better tubing connections, while eliminating fabrication time and failure rate. Although available 3D printable materials are gas-impermeable, the addition of a PDMS membrane following printing of the passive microfluidic network is a simple addition allowing gas transfer. In this case, having a gas-impermeable material for the bulk is advantageous as it reduces unwanted gas transfer from the bulk material prior to the gas exchange interface. The previous PDMS devices were Parylene coated along the convection channels to eliminate exchange of gas from the PDMS bulk, which again added to their complexity and is no longer needed. Convection and distribution of the gas is done in the impermeable material, eliminating dilution of the gas before reaching the diffusion layer.

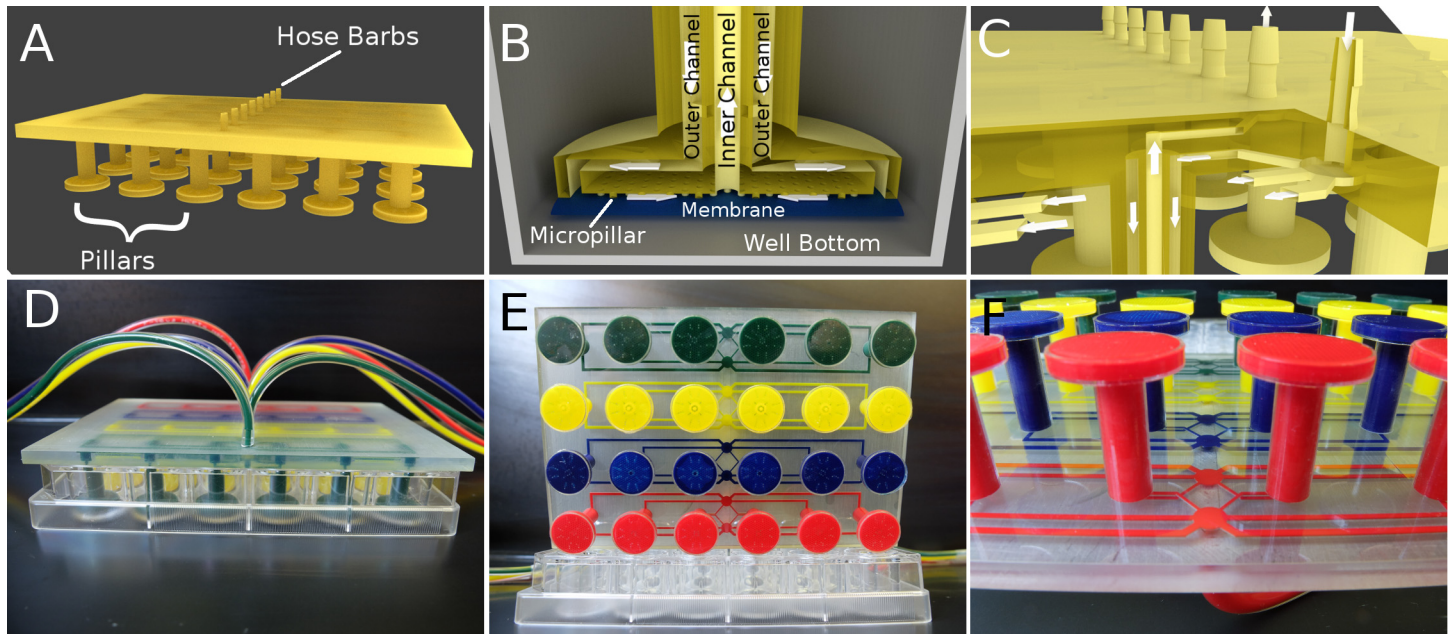


Fig 1. Design of 24-well Insert Device. (A) Rendering of whole 3D printed part. An inlet and outlet barb allows perfusion of gas to control 6 wells. (B) At the bottom of each pillar gas entering from the outer channel flows along the PDMS membrane (blue), which is supported by micropillars, and exhausts via the inner pipe. Diffusion occurs rapidly through the PDMS membrane to the cell culture spaced 500 μm away at the bottom of the well. (C) Cross-section demonstrating how the microfluidic distribution network and double pipes are connected. The two adjacent mirrored distribution networks are spaced 1 mm apart along the z-axis allowing them to overlap and enter the separate vertical pipes. The arrows indicate the flow direction. The incoming gas enters the outer pipe on its way to the bottom of the well and returns through the inner pipe. (D) Photo of the device with dyed channels in a 24-well plate. (E) Photo of the device from the bottom with four independent channel networks. (F) Photo of the printed distribution networks.

doi:10.1371/journal.pone.0137631.g001

Materials and Methods

Design of insert

The device was designed to integrate with a multiwell format, specifically an off-the-shelf 24-well plate. The 24-well plate insert was designed to control gas in 4 rows of 6 wells each. Each of the 4 rows can be controlled independently from an input and also incorporates an integrated distribution network and hose barbs to simplify device operation. The pillars extend into each well leaving a $\sim 500 \mu\text{m}$ gap between the diffusion membrane and the culture surface. This gap allows space for $\sim 0.17 \text{ mL}$ of media. Diffusion occurs rapidly across this gap allowing control of the dissolved gas environment around the cells. A distribution network stems from the central input that equalizes the flow along each path length by varying the channel width to the proximal, intermediate, and distal wells (Fig 1). The device also features a pipe within a pipe design so that gas flow enters and leaves the diffusion area in a uniform, and symmetrical flow pattern, which would not be possible with standard lithography and demonstrates the capabilities of 3D printing (Fig 1).

Fabrication of the insert

CAD models were designed in Autodesk and Blender and printed via stereolithography in Watershed XC by Finline Prototyping. The 3D part contained the microfluidic delivery channels, and was completed by adhering a gas-permeable membrane of PDMS to enable diffusion of gas to the culture area. The PDMS membranes were fabricated by spin coating 10:1 PDMS (Sylgard 184) on a silicon wafer at 900 RPM to a thickness of $\sim 100 \mu\text{m}$ and curing at 70°C for

30 minutes. The PDMS membrane was cut to size and attached to the 3D-printed network with an additional, thin layer of PDMS that was applied as an adhesive to the membrane, secured in position on the end of each pillar, and allowed to cure in place.

Oxygen characterization

Oxygen was measured with PtOEPK (Pt(II) Octaethylporphine ketone) planar sensors that were fixed to the bottom of a 24-well plate. Sensors were prepared as discussed previously [43, 44]. Briefly, polystyrene was dissolved in toluene to form a solution to which PtOEPK (Frontier Scientific) was mixed in before spin coating to a thin layer and allowing the toluene to evaporate. Five calibration points were fitted to a two-site model [45, 46] of the Stern-Volmer relationship which was used to correlate sensor intensities with oxygen concentration.

Gas was pulled through the device with negative pressure as a precaution to avoid bulging or detaching membranes, as well as bubble formation in the culture media. The outlet ports were connected to a water aspirator which pulled gas through the device from the inlet ports via a flow meter (FL-5311G; Omega) set at 50 ccm. The inlet tubing was placed in an open cone that was flooded with gas from a tank with a flow rate of 30 ccm which exceeded the vacuum flow rate (12.5 ccm per 6-well network) so that the gas of interest was pulled into the inlet rather than room air due to the open connection. In this way, the pressure, and therefore flow rate, was equal across the 4 networks without having to balance flow from 4 pressurized sources, yet different gases of interest can be perfused via vacuum.

Initially the inlets are fed with a 5% CO₂, balanced air tank until the intensity stabilized. The inlets were then switched to the control gas of either 0, 5, 10, or 21% O₂, each with 5% CO₂ and balanced with N₂. Intensity measurements were then taken every five minutes for six hours. All gas tanks used in the oxygen characterization were 5% CO₂ in addition to the desired gas mix in anticipation of cell culture experiments (where CO₂ is necessary to buffer the culture media) as CO₂ can alter the fluorescence of the PtOEPK. The this entire procedure was repeated three independent times.

Cell culture

The assembled device was sterilized by spraying with 70% ethanol solution and placed in a biosafety hood with UV lights overnight. Human lung adenocarcinoma (A549) cells were seeded at 30,000 cells per well in a 24-well plate. Cells were cultured in DMEM supplemented with 10% FBS. After reaching ~ 70% confluency, the 24-well insert was placed in the plate and the gases were perfused through the device in the same scheme as in the oxygen characterization. Each row of six wells experienced either 0%, 5%, 10% or 21% O₂, with 5% CO₂ and balanced nitrogen. The assembly was placed in an incubator at 37°C for six hours.

Quantitative PCR

Following six hours of oxygen modulation, the 24-well oxygen control insert was removed and culture media was aspirated. No contamination of the culture was observed. Cells in each well were washed twice with PBS, and 300 μ L of a lysis solution consisting of 10 μ L of β -mercaptoethanol (Sigma Aldrich) per 1 mL of lysis buffer (PureLink RNA Mini Kit; Invitrogen) was added to each well. The lysate from each well was collected as a sample. RNA was extracted according to the PureLink RNA Mini Kit manufacturer's instructions.

Synthesis of cDNA was performed using the High-Capacity cDNA Reverse Transcription Kit (Applied Biosystems), and quantitative PCR was carried out on ABI PRISM 7000 (Applied Biosystems) in 25 μ L reactions using Taqman Gene Expression Assays. Beta-2-microglobulin (B2M) served as the endogenous control for calculations of relative gene expression. Six

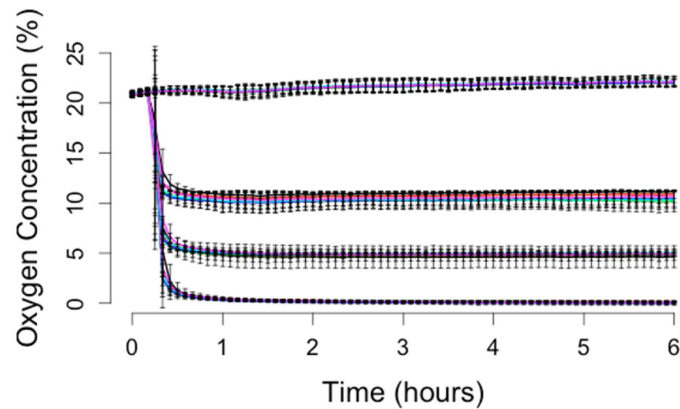


Fig 2. Oxygen Characterization. Time course data of four oxygen conditions are demonstrated in a 24-well plate. Each 6-well row of the plate can be controlled independently. Error bars are the standard deviation $N = 3$.

doi:10.1371/journal.pone.0137631.g002

technical replicates from the 6-well control unit were processed for each of four oxygen conditions (0%, 5%, 10% and 21% O_2) in three independent experiments.

Statistical analysis

Cell culture experiments were repeated three independent times. Data are expressed as the mean \pm SD. One-way ANOVA with Tukey's multiple comparison post-test performed by Prism 5 (Graphpad) determined significance.

Results

Oxygen control

Oxygen control in the 24-well insert device was quantified with a platinum-based (PtOEPK) planar oxygen sensor placed at the bottom of the well, as shown in Fig 2. The device reaches steady state in 30 minutes and can then hold the oxygen level near 0% O_2 indefinitely, while 95% N_2 , 5% CO_2 is pumped through the device. A different gas condition can be used in each separate iteration of the 6-well unit allowing 6 technical replicates of up to 4 different gas conditions in one 24-well plate. There was little variation in the oxygen levels measured in each of the 6 wells controlled by a single inlet, demonstrating the distribution network worked effectively.

Bioverification

Oxygen levels of 21%, 10%, 5%, and 0% were applied to each set of 6 wells in which A549 cells were cultured. Measurement of relative gene expression confirmed biological responsiveness of cells under the device's control. The device's ability to control the gas environment was demonstrated with hypoxia-induced upregulation of VEGFA mRNA in the A549 cells (Fig 3). Quantitative PCR showed a significant increase in the relative gene expression of VEGFA in wells exposed to 0% O_2 for 6 hours as compared to 21% O_2 . Hypoxia-induced alterations in gene expression usually indicate a HIF-transduced hypoxic signal in cells. When a HIF transcription factor undergoes nuclear translocation, it can initiate transcription of genes by binding to the hypoxia response element (HRE) [47] on its target genes. VEGFA has previously been shown to have a functional HRE, and upregulation has been observed in A549 cells under hypoxic

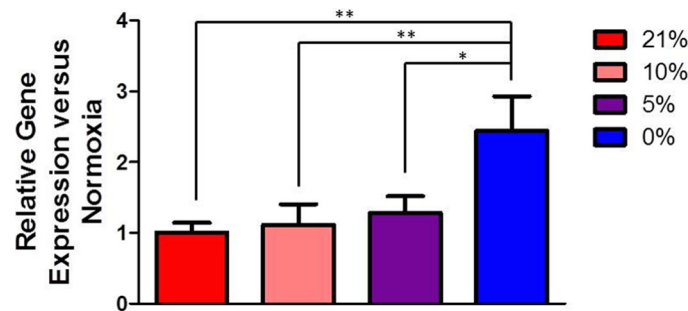


Fig 3. PCR Data. VEGFA expression in A549 cells after exposure to different oxygen conditions set-up by the insert device. Data are expressed as mean \pm SD, N = 3.

doi:10.1371/journal.pone.0137631.g003

conditions [48]. The 6 h time point was chosen based on the HIF-1 α timecourse in A549 cells. HIF-1 α protein levels are maximal at 4 h and steeply decrease by 16 h [49]. Based on the known time course, we looked at a time point slightly delayed from the 4 h peak to account for transcription of the downstream target genes.

Discussion

This new iteration of the multi-well insert for oxygen control maintains the convenient features of the previous design while improving distribution and interfacing with tubing due to the 3D-printed element. Oxygen control is performed in an off-the-shelf culture plate allowing standard protocols to be used for analysis assays or imaging where additional protocols are often required when cells are seeded within microfluidic chips. The VEGFA gene expression in A549 cells confirms a biological response using the multi-well insert.

This 3D-printed device improves on our previous design in a number of ways. First, the fabrication is greatly simplified. No microfabrication, PDMS molding or Parylene coating is required. Additionally, the non-permanent adhesion of membranes to the 3D-part allow them to be removed and replaced if they are damaged. In PDMS devices the layers are bonded permanently via plasma bonding so damage to a membrane is not repairable. 3D-printing also enables higher levels of intricacy without any additional fabrication, allowing us to include the distribution network, overlapping of channels in the z-axis, and the ‘pipe within a pipe’ design. A comparable PDMS device would require several additional microfabricated layers to be manually aligned to reproduce just the distribution network.

Moving forward with additive manufacturing of microfluidic devices is desirable as it will enable highly integrated designs without any additional fabrication. For this device an in-device gas mixer could allow more conditions in a single plate, perhaps even one per well or even gradients within wells while reducing the number of gas tanks required as inputs. This design could also be applied to higher format plates such as 96-well plates.

Conclusion

3D printing microfluidic chips have been limited to oxygen-impermeable materials. We demonstrate oxygen control in 3D-printed devices with the addition of a gas permeable PDMS membrane. Oxygen control is demonstrated in a 24-well plate and PCR detection of upregulation of VEGFA mRNA in A549 cells shows the device effectively controls oxygen as expected. 3D printing allows complex designs, integrated tubing connectors, and is comparable in price to standard PDMS fabrication. This technique represents a bridge to commercialization where

robust devices can be more easily shared and disseminated. While injection molding, hot embossing, or other industrial processes are cheaper when making hundreds to thousands of devices, it is not practical to make an injection mold when making tens to hundreds of devices. In addition, PDMS fabrication would be too time consuming, expensive, and the failure rate would be unacceptable. 3D printing is an excellent solution to these device fabrication needs.

Supporting Information

S1 Dataset. Oxygen Characterization Dataset. This dataset consists of intensity values of the oxygen sensors as well as the analyzed oxygen values.

(ZIP)

S2 Dataset. VEGF Dataset. This dataset consists of quantitative real-time PCR for genes VEGFA and B2M.

(XLSX)

Author Contributions

Conceived and designed the experiments: MDB MLR DTE. Performed the experiments: MDB MLR. Analyzed the data: MDB MLR. Contributed reagents/materials/analysis tools: MDB MLR DTE. Wrote the paper: MDB MLR DTE.

References

1. Oppegard SC, Nam KH, Carr JR, Skaalure SC, Eddington DT. Modulating temporal and spatial oxygenation over adherent cellular cultures. *PLoS ONE*. 2009; 4(9). doi: [10.1371/journal.pone.0006891](https://doi.org/10.1371/journal.pone.0006891) PMID: [19727397](https://pubmed.ncbi.nlm.nih.gov/19727397/)
2. Oppegard SC, Blake AJ, Williams JC, Eddington DT. Precise control over the oxygen conditions within the Boyden chamber using a microfabricated insert. *Lab on a chip*. 2010 Sep; 10(18):2366–73. Available from: <http://www.ncbi.nlm.nih.gov/pubmed/20689862> doi: [10.1039/c004856a](https://doi.org/10.1039/c004856a) PMID: [20689862](https://pubmed.ncbi.nlm.nih.gov/20689862/)
3. Waldbaur A, Rapp H, Länge K, Rapp BE. Let there be chip—towards rapid prototyping of microfluidic devices: one-step manufacturing processes. *Analytical Methods*. 2011; 3(12):2681. Available from: <http://xlink.rsc.org/?DOI=c1ay05253e> doi: [10.1039/c1ay05253e](https://doi.org/10.1039/c1ay05253e)
4. Chen C, Erkal JL, Gross BC, Lockwood SY, Spence DM. Evaluation of 3D Printing and Its Potential Impact on Biotechnology and the Chemical Sciences. *Analytical Chemistry*. 2014; 86:3240–3253. doi: [10.1021/ac403397r](https://doi.org/10.1021/ac403397r) PMID: [24432804](https://pubmed.ncbi.nlm.nih.gov/24432804/)
5. Au AK, Lee W, Folch A. Mail-order microfluidics: evaluation of stereolithography for the production of microfluidic devices. *Lab on a chip*. 2014 Apr; 14(7):1294–301. Available from: <http://www.ncbi.nlm.nih.gov/pubmed/24510161> doi: [10.1039/c3lc51360b](https://doi.org/10.1039/c3lc51360b) PMID: [24510161](https://pubmed.ncbi.nlm.nih.gov/24510161/)
6. Comina G, Suska A, Filippini D. Low cost lab-on-a-chip prototyping with a consumer grade 3D printer. *Lab on a chip*. 2014; 14:2978–2982. Available from: <http://www.ncbi.nlm.nih.gov/pubmed/24931176> doi: [10.1039/C4LC00394B](https://doi.org/10.1039/C4LC00394B) PMID: [24931176](https://pubmed.ncbi.nlm.nih.gov/24931176/)
7. Chen C, Wang Y, Lockwood SY, Spence DM. 3D-printed fluidic devices enable quantitative evaluation of blood components in modified storage solutions for use in transfusion medicine. *The Analyst*. 2014 Jun; 139(13):3219–26. Available from: <http://pubs.rsc.org/en/content/articlehtml/2014/an/c3an02357e> doi: [10.1039/C3AN02357E](https://doi.org/10.1039/C3AN02357E) PMID: [24660218](https://pubmed.ncbi.nlm.nih.gov/24660218/)
8. Shallan AI, Smejkal P, Corban M, Guijt RM, Breadmore MC. Cost-effective three-dimensional printing of visibly transparent microchips within minutes. *Analytical Chemistry*. 2014; 86:3124–3130. doi: [10.1021/ac4041857](https://doi.org/10.1021/ac4041857) PMID: [24512498](https://pubmed.ncbi.nlm.nih.gov/24512498/)
9. Bhargava KC, Thompson B, Malmstadt N. Discrete elements for 3D microfluidics. *Proceedings of the National Academy of Sciences*. 2014; 111(42):15013–15018. Available from: <http://www.pnas.org/lookup/doi/10.1073/pnas.1414764111> doi: [10.1073/pnas.1414764111](https://doi.org/10.1073/pnas.1414764111)
10. Yuen PK. SmartBuild—a truly plug-n-play modular microfluidic system. *Lab on a chip*. 2008; 8(8):1374–1378. doi: [10.1039/b805086d](https://doi.org/10.1039/b805086d) PMID: [18651081](https://pubmed.ncbi.nlm.nih.gov/18651081/)
11. Lee KG, Park KJ, Seok S, Shin S, Kim DH, Park JY, et al. 3D printed modules for integrated microfluidic devices. *RSC Advances*. 2014;p. 32876–32880. Available from: <http://pubs.rsc.org/en/content/articlehtml/2014/ra/c4ra05072j> doi: [10.1039/C4RA05072J](https://doi.org/10.1039/C4RA05072J)

12. Tek P, Chiganos TC, Mohammed JS, Eddington DT, Fall CP, Ifft P, et al. Rapid prototyping for neuroscience and neural engineering. *Journal of Neuroscience Methods*. 2008; 172:263–269. doi: [10.1016/j.jneumeth.2008.03.011](https://doi.org/10.1016/j.jneumeth.2008.03.011) PMID: [18565590](https://pubmed.ncbi.nlm.nih.gov/18565590/)
13. Kitson PJ, Rosnes MH, Sans V, Dragone V, Cronin L. Configurable 3D-Printed millifluidic and microfluidic 'lab on a chip' reactionware devices. *Lab on a Chip*. 2012; 12(18):3267. doi: [10.1039/c2lc40761b](https://doi.org/10.1039/c2lc40761b) PMID: [22875258](https://pubmed.ncbi.nlm.nih.gov/22875258/)
14. Symes MD, Kitson PJ, Yan J, Richmond C, Cooper GJT, Bowman RW, et al. Integrated 3D-printed reactionware for chemical synthesis and analysis. *Nature Chemistry*. 2012; 4(5):349–354. Available from: <http://eprints.gla.ac.uk/68744/> doi: [10.1038/nchem.1313](https://doi.org/10.1038/nchem.1313) PMID: [22522253](https://pubmed.ncbi.nlm.nih.gov/22522253/)
15. Kitson PJ, Symes MD, Dragone V, Cronin L. Combining 3D printing and liquid handling to produce user-friendly reactionware for chemical synthesis and purification. *Chemical Science*. 2013; 4:3099–3103. Available from: <http://dx.doi.org/10.1039/c3sc51253c> doi: [10.1039/C3SC51253C](https://doi.org/10.1039/C3SC51253C)
16. Kitson PJ, Marshall RJ, Long D, Forgan RS, Cronin L. 3D Printed high-throughput hydrothermal reactionware for discovery, optimization, and scale-up. *Angewandte Chemie—International Edition*. 2014; p. 1–7.
17. Busch W, Moore BT, Martsberger B, Mace DL, Twigg RW, Jung J, et al. A microfluidic device and computational platform for high-throughput live imaging of gene expression. *Nature Methods*. 2012; 9(11). doi: [10.1038/nmeth.2185](https://doi.org/10.1038/nmeth.2185) PMID: [23023597](https://pubmed.ncbi.nlm.nih.gov/23023597/)
18. Erkal JL, Selimovic A, Gross BC, Lockwood SY, Walton EL, McNamara S, et al. 3D printed microfluidic devices with integrated versatile and reusable electrodes. *Lab on a chip*. 2014; 14:2023–32. Available from: <http://www.ncbi.nlm.nih.gov/pubmed/24763966> doi: [10.1039/c4lc00171k](https://doi.org/10.1039/c4lc00171k) PMID: [24763966](https://pubmed.ncbi.nlm.nih.gov/24763966/)
19. Lee W, Kwon D, Chung B, Jung GY, Au A, Folch A, et al. Ultrarapid detection of pathogenic bacteria using a 3D immunomagnetic flow assay. *Analytical Chemistry*. 2014; 86(13):6683–6688. doi: [10.1021/ac501436d](https://doi.org/10.1021/ac501436d) PMID: [24856003](https://pubmed.ncbi.nlm.nih.gov/24856003/)
20. Lee W, Kwon D, Choi W, Jung GY, Jeon S. 3D-Printed Microfluidic Device for the Detection of Pathogenic Bacteria Using Size-based Separation in Helical Channel with Trapezoid Cross-Section. *Scientific Reports*. 2015; 5:7717. Available from: <http://www.nature.com/doi/10.1038/srep07717> doi: [10.1038/srep07717](https://doi.org/10.1038/srep07717) PMID: [25578942](https://pubmed.ncbi.nlm.nih.gov/25578942/)
21. Au AK, Bhattacharjee N, Horowitz LF, Chang TC, Folch A. 3D-Printed Microfluidic Automation. *Lab Chip*. 2015;p. 1–8. Available from: <http://pubs.rsc.org/en/Content/ArticleLanding/2015/LC/C5LC00126A>
22. Causier A, Carret G, Boutin C, Berthelot T, Berthault P. 3D-printed system optimizing dissolution of hyperpolarized gaseous species for micro-sized NMR. *Lab Chip*. 2015; Available from: <http://pubs.rsc.org/en/Content/ArticleLanding/2015/LC/C5LC00193E> doi: [10.1039/C5LC00193E](https://doi.org/10.1039/C5LC00193E) PMID: [25805248](https://pubmed.ncbi.nlm.nih.gov/25805248/)
23. Chi A, Curi S, Clayton K, Luciano D, Klauber K, Alexander-Katz A, et al. Rapid Reconstitution Packages (RRPs) implemented by integration of computational fluid dynamics (CFD) and 3D printed microfluidics. *Drug Delivery and Translational Research*. 2014; 4(4):320–333. Available from: <http://link.springer.com/10.1007/s13346-014-0198-7> doi: [10.1007/s13346-014-0198-7](https://doi.org/10.1007/s13346-014-0198-7) PMID: [25787065](https://pubmed.ncbi.nlm.nih.gov/25787065/)
24. Chisholm G, Kitson PJ, Kirkaldy ND, Bloor LG, Cronin L. 3D printed flow plates for the electrolysis of water. *Energy & Environmental Science*. 2014; 7(iii):3026–3032. Available from: <http://dx.doi.org/10.1039/C4EE01426J> doi: [10.1039/C4EE01426J](https://doi.org/10.1039/C4EE01426J)
25. McDonald JC, Chabinyc ML, Metallo SJ, Anderson JR, Stroock AD, Whitesides GM. Prototyping of Microfluidic Devices in Poly (dimethylsiloxane) Using Solid-Object Printing the fabrication of microfluidic devices in poly (dimethyl-). *Analytical chemistry*. 2002; 74(7):1537–1545. doi: [10.1021/ac010938q](https://doi.org/10.1021/ac010938q) PMID: [12033242](https://pubmed.ncbi.nlm.nih.gov/12033242/)
26. Gregory C, Veeman M. 3D-printed microwell arrays for Ciona microinjection and timelapse imaging. *PLoS ONE*. 2013; 8(12):8–13. doi: [10.1371/journal.pone.0082307](https://doi.org/10.1371/journal.pone.0082307)
27. King PH, Jones G, Morgan H, de Planque MRR, Zauner KP. Interdroplet bilayer arrays in millifluidic droplet traps from 3D-printed moulds. *Lab on a chip*. 2014; 14(4):722–9. Available from: <http://www.ncbi.nlm.nih.gov/pubmed/24336841> doi: [10.1039/C3LC51072G](https://doi.org/10.1039/C3LC51072G) PMID: [24336841](https://pubmed.ncbi.nlm.nih.gov/24336841/)
28. Comina G, Suska A, Filippini D. PDMS lab-on-a-chip fabrication using 3D printed templates. *Lab on a chip*. 2014; 14:424–30. Available from: <http://www.ncbi.nlm.nih.gov/pubmed/24281262> doi: [10.1039/C3LC50956G](https://doi.org/10.1039/C3LC50956G) PMID: [24281262](https://pubmed.ncbi.nlm.nih.gov/24281262/)
29. Kamei Ki, Mashimo Y, Koyama Y, Fockenberg C, Nakashima M, Nakajima M, et al. 3D printing of soft lithography mold for rapid production of polydimethylsiloxane-based microfluidic devices for cell stimulation with concentration gradients. *Biomedical Microdevices*. 2015; 17(2). Available from: <http://link.springer.com/10.1007/s10544-015-9928-y> doi: [10.1007/s10544-015-9928-y](https://doi.org/10.1007/s10544-015-9928-y) PMID: [25686903](https://pubmed.ncbi.nlm.nih.gov/25686903/)
30. Therriault D, White SR, Lewis JA. Chaotic mixing in three-dimensional microvascular networks fabricated by direct-write assembly. *Nature materials*. 2003 Apr; 2(4):265–71. Available from: <http://dx.doi.org/10.1038/nmat863> doi: [10.1038/nmat863](https://doi.org/10.1038/nmat863) PMID: [12690401](https://pubmed.ncbi.nlm.nih.gov/12690401/)

31. Miller JS, Stevens KR, Yang MT, Baker BM, Nguyen DHT, Cohen DM, et al. Rapid casting of patterned vascular networks for perfusable engineered three-dimensional tissues. *Nature materials*. 2012 Sep; 11(9):768–74. Available from: <http://www.pubmedcentral.nih.gov/articlerender.fcgi?artid=3586565&tool=pmcentrez&rendertype=abstract> doi: [10.1038/nmat3357](https://doi.org/10.1038/nmat3357) PMID: [22751181](https://pubmed.ncbi.nlm.nih.gov/22751181/)
32. Bhargava R, Gelber MK. Monolithic Multilayer Microfluidics via Sacrificial Molding of 3D-Printed Iso-malt. *Lab Chip*. 2015; 15:1736–1741. Available from: <http://pubs.rsc.org/en/Content/ArticleLanding/2015/LC/C4LC01392A> doi: [10.1039/c4lc01392a](https://doi.org/10.1039/c4lc01392a) PMID: [25671493](https://pubmed.ncbi.nlm.nih.gov/25671493/)
33. Femmer T, Kuehne a, Wessling M. Print your own membrane: Direct rapid prototyping of polydimethylsiloxane. *Lab on a Chip*. 2014; 14:2610–2613. Available from: <http://pubs.rsc.org/en/content/articlehtml/2014/lc/c4lc00320a> doi: [10.1039/c4lc00320a](https://doi.org/10.1039/c4lc00320a) PMID: [24828586](https://pubmed.ncbi.nlm.nih.gov/24828586/)
34. Sia SK, Whitesides GM. Microfluidic devices fabricated in poly(dimethylsiloxane) for biological studies. *Electrophoresis*. 2003; 24(21):3563–3576. doi: [10.1002/elps.200305584](https://doi.org/10.1002/elps.200305584) PMID: [14613181](https://pubmed.ncbi.nlm.nih.gov/14613181/)
35. Brennan MD, Rexus-Hall ML, Elgass LJ, Eddington DT. Oxygen control with microfluidics. *Lab Chip*. 2014; 14(22):4305–4318. Available from: <http://xlink.rsc.org/?DOI=C4LC00853G> doi: [10.1039/C4LC00853G](https://doi.org/10.1039/C4LC00853G) PMID: [25251498](https://pubmed.ncbi.nlm.nih.gov/25251498/)
36. Kumar V, Gabrilovich DI. Hypoxia-inducible factors in regulation of immune responses in tumour micro-environment. *Immunology*. 2014; 143(4):512–519. Available from: <http://doi.wiley.com/10.1111/imm.12380> doi: [10.1111/imm.12380](https://doi.org/10.1111/imm.12380) PMID: [25196648](https://pubmed.ncbi.nlm.nih.gov/25196648/)
37. Vaupel P, Harrison L. Tumor hypoxia: causative factors, compensatory mechanisms, and cellular response. *The oncologist*. 2004 Jan; 9 Suppl 5(Supplement 5):4–9. Available from: http://theoncologist.alphamedpress.org/content/9/suppl_5/4.full doi: [10.1634/theoncologist.9-90005-4](https://doi.org/10.1634/theoncologist.9-90005-4) PMID: [15591417](https://pubmed.ncbi.nlm.nih.gov/15591417/)
38. Vaupel P, Mayer A. Hypoxia in cancer: significance and impact on clinical outcome. *Cancer metastasis reviews*. 2007 Jun; 26(2):225–39. Available from: <http://www.ncbi.nlm.nih.gov/pubmed/17440684> doi: [10.1007/s10555-007-9055-1](https://doi.org/10.1007/s10555-007-9055-1) PMID: [17440684](https://pubmed.ncbi.nlm.nih.gov/17440684/)
39. Gilkes DM, Semenza GL, Wirtz D. Hypoxia and the extracellular matrix: drivers of tumour metastasis. *Nature reviews Cancer*. 2014 Jun; 14(6):430–9. Available from: <http://dx.doi.org/10.1038/nrc3726> doi: [10.1038/nrc3726](https://doi.org/10.1038/nrc3726) PMID: [24827502](https://pubmed.ncbi.nlm.nih.gov/24827502/)
40. Ke Q, Costa M. Hypoxia-inducible factor-1 (HIF-1). *Molecular pharmacology*. 2006 Nov; 70(5):1469–80. Available from: <http://molpharm.aspetjournals.org/content/70/5/1469.full> doi: [10.1124/mol.106.027029](https://doi.org/10.1124/mol.106.027029) PMID: [16887934](https://pubmed.ncbi.nlm.nih.gov/16887934/)
41. Semenza GL. Regulation of mammalian O₂ homeostasis by hypoxia-inducible factor 1. *Annual review of cell and developmental biology*. 1999 Jan; 15:551–78. Available from: <http://www.annualreviews.org/doi/abs/10.1146/annurev.cellbio.15.1.551> doi: [10.1146/annurev.cellbio.15.1.551](https://doi.org/10.1146/annurev.cellbio.15.1.551) PMID: [10611972](https://pubmed.ncbi.nlm.nih.gov/10611972/)
42. Semenza G. Signal transduction to hypoxia-inducible factor 1. *Biochemical pharmacology*. 2002 Sep; 64(5-6):993–8. Available from: <http://www.ncbi.nlm.nih.gov/pubmed/12213597> doi: [10.1016/S0006-2952\(02\)01168-1](https://doi.org/10.1016/S0006-2952(02)01168-1) PMID: [12213597](https://pubmed.ncbi.nlm.nih.gov/12213597/)
43. Sinkala E, Eddington DT. Oxygen sensitive microwells. *Lab on a chip*. 2010 Dec; 10(23):3291–5. Available from: <http://pubs.rsc.org/en/Content/ArticleHTML/2010/LC/C0LC00244E> doi: [10.1039/c0lc00244e](https://doi.org/10.1039/c0lc00244e) PMID: [20938500](https://pubmed.ncbi.nlm.nih.gov/20938500/)
44. Rexus-Hall ML, Mauleon G, Malik AB, Rehman J, Eddington DT. Microfluidic platform generates oxygen landscapes for localized hypoxic activation. *Lab on a chip*. 2014 Dec; 14(24):4688–95. Available from: <http://www.ncbi.nlm.nih.gov/pubmed/25315003> doi: [10.1039/c4lc01168f](https://doi.org/10.1039/c4lc01168f) PMID: [25315003](https://pubmed.ncbi.nlm.nih.gov/25315003/)
45. Carraway ER, Demas JN, DeGraff Ba, Bacon JR. Photophysics and photochemistry of oxygen sensors based on luminescent transition-metal complexes. *Analytical Chemistry*. 1991; 63(4):337–342. Available from: <http://dx.doi.org/10.1021/ac00004a007> doi: [10.1021/ac00004a007](https://doi.org/10.1021/ac00004a007)
46. Wang Xd, Wolfbeis OS. Optical methods for sensing and imaging oxygen: materials, spectroscopies and applications. *Chemical Society reviews*. 2014; 43(10):3666–761. Available from: <http://www.ncbi.nlm.nih.gov/pubmed/24638858> doi: [10.1039/C4CS00039K](https://doi.org/10.1039/C4CS00039K) PMID: [24638858](https://pubmed.ncbi.nlm.nih.gov/24638858/)
47. Lee JW, Bae SH, Jeong JW, Kim SH, Kim KW. Hypoxia-inducible factor (HIF-1)alpha: its protein stability and biological functions. *Experimental & molecular medicine*. 2004 Feb; 36(1):1–12. Available from: <http://www.ncbi.nlm.nih.gov/pubmed/15031665> doi: [10.1038/emmm.2004.1](https://doi.org/10.1038/emmm.2004.1)
48. Rohrer Bley C, Orlowski K, Furmanova P, McSheehy PMJ, Pruschy M. Regulation of VEGF-expression by patupilone and ionizing radiation in lung adenocarcinoma cells. *Lung cancer (Amsterdam, Netherlands)*. 2011 Sep; 73(3):294–301. Available from: <http://www.sciencedirect.com/science/article/pii/S0169500211000468> doi: [10.1016/j.lungcan.2011.01.010](https://doi.org/10.1016/j.lungcan.2011.01.010)
49. Li QF, Wang XR, Yang YW, Lin H. Hypoxia upregulates hypoxia inducible factor (HIF)-3alpha expression in lung epithelial cells: characterization and comparison with HIF-1alpha. *Cell research*. 2006; 16(6):548–558. doi: [10.1038/sj.cr.7310072](https://doi.org/10.1038/sj.cr.7310072) PMID: [16775626](https://pubmed.ncbi.nlm.nih.gov/16775626/)